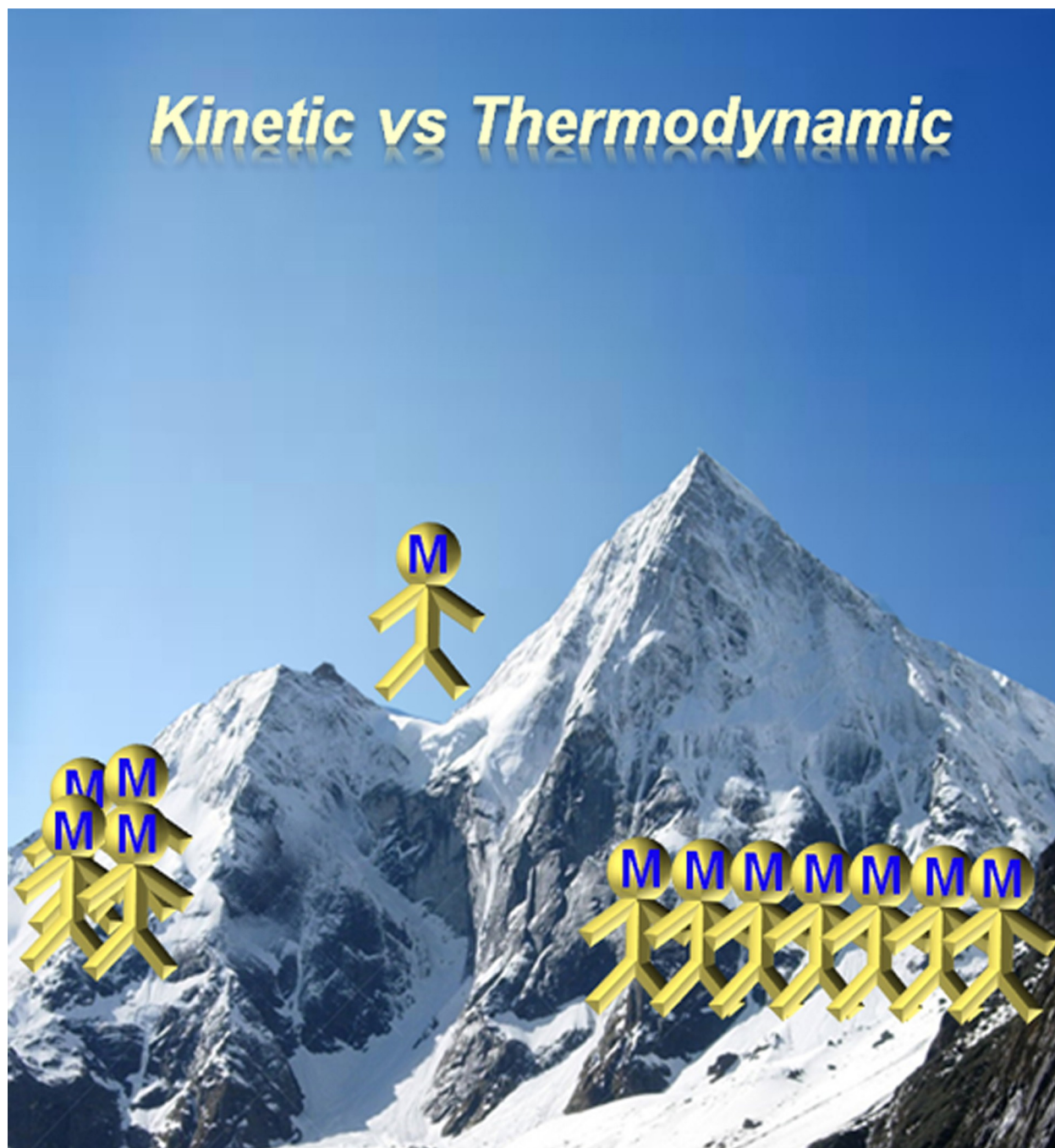


# Controlled Supramolecular Polymerization of $d^8$ Metal Complexes through Pathway Complexity and Seeded Growth

Goutam Ghosh, Tanwistha Ghosh, and Gustavo Fernández\*<sup>[a]</sup>



In recent years, pathway complexity has been studied in detail for a large variety of organic and  $\pi$ -conjugated molecules. However, such investigations on their metal-containing analogues have received only little attention to date, despite the well-known potential of metal complexes in various fields. In this Minireview, we have collected recent examples of  $d^8$  metal complexes (Pt(II), Pd(II) and Au(III) complexes) exhibiting

controlled supramolecular polymerization through pathway complexity and seeded-growth approaches. Controlling the competing thermodynamic vs. kinetic pathways in these systems should help develop advanced metallosupramolecular functional materials with excellent photophysical, electronic, magnetic, catalytic, and biomedical applications.


## Introduction

Supramolecular self-assembly is an impeccably powerful tool to construct highly sophisticated multi-functional artificial systems with tailored properties and applications in all spheres of life ranging from optoelectronic materials to biomaterials.<sup>[1–2]</sup> Inspired by nature's assembly principles, multiple researchers have exploited various non-covalent interactions such as hydrogen bonding, aromatic, electrostatic, dipole-dipole, donor-acceptor or hydrophobic interactions to achieve functionality in such artificial systems.<sup>[1–2]</sup> For a long time, research on self-assembly and supramolecular polymerization has taken for granted that the majority of assemblies of artificial molecules operate under thermodynamic control, thereby overlooking the possible kinetic processes that can also occur. However, the recent advancement of analytical tools as well as the development of kinetic models and simulations have led to an increasing interest in understanding the relationship between thermodynamics and kinetics in self-assembly processes. One of the key early examples where kinetics were observed to play a role in self-assembly processes was reported over two decades ago by Meijer and co-workers.<sup>[3]</sup> In this manuscript, two chiral forms of thin films of optically active regioregular 3-substituted polythiophene were identified in CD experiments depending on whether fast or slow cooling was applied. The stereomutation in the polymer was the outcome of a kinetically favoured metastable state from fast cooling, while the thermodynamically stable state was obtained on slow cooling. Later in 2006, the same group monitored spectroscopically a nucleation process in the hierarchical self-assembly of an oligo-*p*-phenylenevinylene (OPV) driven by aromatic and hydrogen bonding interactions.<sup>[4]</sup> Even though in this pioneering example the authors mostly focused on the thermodynamic aspects of the self-assembly, later studies by the same group brought to light the key implications of kinetics in supramolecular polymerization.<sup>[5]</sup> In fact, careful re-investigation of the system by detailed time-dependent spectroscopic studies and kinetic model calculations demonstrated the presence of two competing pathways -one kinetic and the other thermodynamic. This

phenomenon, termed by the authors as pathway complexity, marked a milestone in the field of self-assembly and encouraged multiple researchers to scrutinize self-assembled systems by considering both kinetic and thermodynamic aspects. In recent years, detailed mechanistic studies of multiple types of self-assembling units have contributed to a rapid development of the field of controlled supramolecular polymerization. In this context, the introduction of the concept of living supramolecular polymerization (LSP)<sup>[6]</sup> represented a clear breakthrough in the field, as this method enabled length and polydispersity control of supramolecular polymers (SP). A main requirement for LSP to be applicable to a given system is the existence of a kinetically controlled state that retards the formation of the thermodynamically controlled species. If seeds of the thermodynamic species are sequentially added to the kinetic state (which can either be an aggregate or a "dormant" monomer state),<sup>[7]</sup> the transformation can be accelerated, leading to SP of controlled length. Typically, control over competing aggregation pathways of a given artificial molecule can be primarily achieved by optimization of sample preparation protocols,<sup>[8]</sup> or by modulation of temperature,<sup>[9]</sup> solvent geometry,<sup>[10]</sup> and by application of external stimuli.<sup>[11]</sup> Alternatively, the energy landscape of a given assembly can also be controlled by fine tuning of the chemical information encoded into the monomers.<sup>[6,7,12,13]</sup> However, predicting and controlling competing aggregation pathways by molecular design represents a major challenge in the field of self-assembly, as evident from the limited amount of literature dealing with this topic. For a comprehensive overview of the recent advances in the field of kinetic vs. thermodynamic self-assembly process, we refer the readers to recent reviews by the groups of Würthner,<sup>[14]</sup> Perrier,<sup>[15]</sup> Meijer,<sup>[16]</sup> Fernández and Sánchez,<sup>[17]</sup> and de Greef and Hermans.<sup>[18]</sup>

To date, thorough studies to unravel the interplay between kinetics and thermodynamics in self-assembled systems have almost exclusively focused on purely organic  $\pi$ -conjugated systems. Such investigations for metal-containing supramolecular homologs (e.g.  $d^8$  complexes), better known as metallosupramolecular polymers (MSPs), have remained limited. This is surprising considering that MSPs arising from metal ion-directed self-assembly offer well-defined coordination geometries, interconversion between different oxidation states, a wide range of binding strength or ligand-exchange kinetics among others.<sup>[19]</sup> Additionally, the use of metal ions in the molecular design provides access to catalytic, magnetic, electrochemical and photochemical properties.<sup>[20]</sup> The size, shape, degree of preorganization, sterics and electronic properties of the selected ligands represent key elements that govern the

[a] Dr. G. Ghosh, Dr. T. Ghosh, Prof. Dr. G. Fernández  
Organisch-Chemisches Institut  
Westfälische Wilhelms-Universität, Münster  
Correnstraße, 40, 48149 Münster (Germany)  
E-mail: fernandg@uni-muenster.de

 © 2020 The Authors. Published by Wiley-VCH Verlag GmbH & Co. KGaA. This is an open access article under the terms of the Creative Commons Attribution Non-Commercial License, which permits use, distribution and reproduction in any medium, provided the original work is properly cited and is not used for commercial purposes.

stacking into ordered self-assembled structures. Additionally, the relative spatial arrangement of the metal ion relative to the ligand as well as steric and electronic effects associated with the existing metal-ligand interaction determine the final property of the supramolecular polymer. Thus, MSPs find numerous applications in diverse fields like sensors, light-emitting diodes, drug delivery, memory devices, and many others.<sup>[21]</sup> In this context, square-planar  $d^8$  transition metal complexes are particularly relevant due to their superior optoelectronic properties associated with their ability to exhibit aromatic and metal-metal interactions.<sup>[21b,22]</sup>

Although the self-assembly of metal complexes has been investigated extensively, particularly for Pt(II) complexes featuring tridentate ligands,<sup>[21b,22,23]</sup> reports dealing with controlled supramolecular polymerization of kinetic vs. thermodynamic aggregates remain limited. In this review, we have collated recent reports on controlled supramolecular polymerization of  $d^8$  metal complexes [Pt(II), Pd(II) and Au(III)] that have been observed to undergo pathway complexity and/or seeded growth. In the following, these systems will be classified depending on the type of ligands used to complex the Pd(II) or Pt(II) or Au(III) ions, such as tridentate (pyridine bis-triazole/tetrazole, terpyridine and cyclometalating) and monodentate (pyridine) ligands.

#### A. $d^8$ metal complexes based on tridentate ligands

$d^8$  metal complexes containing tridentate ligands are by far the most commonly investigated square-planar metal complexes in terms of self-assembly due to their interesting photophysical behavior, e.g. luminescence, and their proven ability to form metal-metal and  $\pi$ - $\pi$  interactions. In this section, we will describe systems exhibiting pathway complexity and/or seeded growth based on a variety of ligands, such as terpyridine, pyridine bis-tetrazole, pyridine bis-triazole, pyridine benzimida-

zole,  $[M(N^A N^A N)L]^n+$  ( $n=1$  or  $2$ ;  $L$ =anionic or neutral ligand) and cyclometalating ligands ( $N^A C^A N$  and  $C^A N^A N$ ).

#### A.1. Pyridine bis-tetrazole ligands

In 2015, Manners and co-workers reported for the first time length control of supramolecular polymers based on square-planar Pt(II) metal complexes.<sup>[24]</sup> In this seminal work, a Pt(II) complex **1** ( $n=16$ ; Figure 1a) containing a tridentate pyridine bis-tetrazole  $N^A N^A N$  ligand and an oligo(ethyleneglycol) (OEG)-functionalized pyridyl ancillary ligand was studied. This system was observed to assemble into well-defined block co-micelles with segmented structures by living crystallization driven self-assembly (CDSA). Complex **1** forms kinetically trapped polydisperse ( $L_w/L_n=1.73$ ) fibers in different organic solvents such as  $CHCl_3$ , DMF and  $CH_3CN$  upon aging for 24 h at  $21^\circ C$ . The length of the fibers remains almost unchanged even after aging the solution for 3 days. To control the fiber length, initially small fiber seeds were prepared by gentle sonication of a solution of polydisperse fibers of **1** in  $CHCl_3$  at  $0^\circ C$  for 1 h. Subsequently, different amounts of molecularly dissolved **1** (unimer) in  $CH_3CN$  at  $80^\circ C$  were added to the solution of fiber seeds of **1** in  $CHCl_3$  and incubated at  $21^\circ C$  for 24 h prior to drop cast. Transmission electron microscopy (TEM) images revealed a linear dependence of the average contour length ( $L_n$ ) on the unimer to seed mass ratio (Figure 1d–g) in a manner analogous to a living covalent polymerization of molecular monomers with a low polydispersity ( $L_w/L_n=1.14$ ).

As a follow-up to this work,<sup>[25]</sup> the authors have investigated how the dynamic behavior and dimensions of the supramolecular polymers are affected upon varying the OEG chain length. For that purpose, they synthesized two new Pt(II) complexes **2** and **3** where the OEG chain was increasingly shortened compared to **1** (**2**,  $n=12$ ; **3**,  $n=7$ ; Figure 1a). In analogy to **1**, **2** and **3** also form initially 1D nanofibers under the



Goutam Ghosh received his Ph.D. in December 2014 from University of Calcutta, Kolkata (India) under the supervision of Prof. Dipak K. Mandal. After his PhD, he joined the group Prof. Suhrit Ghosh at the Indian Association for the Cultivation of Science (IACS), Kolkata as postdoctoral researcher working on controlled supramolecular polymerization and peptide self-assembly. In April 2019, he joined the group of Prof. Gustavo Fernández at the Westfälische Wilhelms Universität (WWU) Münster as a postdoctoral researcher. Currently he is working on supramolecular polymerization of metal complexes based on peptide-functionalized ligands.



Tanwistha Ghosh received her Ph.D. from the AcSIR - Academy of Scientific & Innovative Research at CSIR-NIIST, Thiruvananthapuram, India in 2019 under the supervision of Dr. Vijayakumar C. Nair for work on Thiophene oligomers for photovoltaic applications. Soon after obtaining her PhD degree, she received a WWU fellowship to work as a Visiting Scholar in the group of Prof. Dr. Gustavo Fernández at the WWU Münster. Her work focused on the development of donor-acceptor metallosupramolecular polymers.



Gustavo Fernández is Professor of Organic and Supramolecular Chemistry at the WWU Münster (Germany) since 2015, where he heads a research group working on supramolecular functional materials. His research focuses on understanding the structure-property relationship in (stimuli-responsive) supramolecular assemblies of metal-containing  $\pi$ -systems and BODIPY dyes.

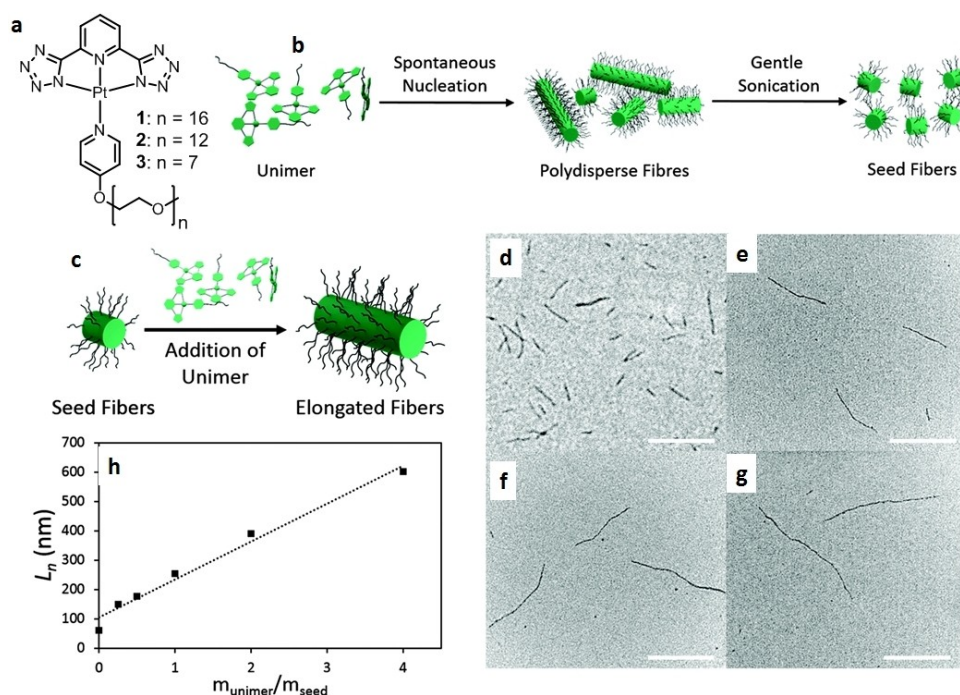


**Figure 1.** a) Chemical structures of 1–3; Schematic representation of the formation of fibers (b) and elongated fibers (c) from 1; TEM micrographs of: d) seed fibers ( $L_n = 60$  nm,  $L_w/L_n = 1.14$ ) formed through gentle sonication of polydisperse fibers; e–f) elongated fibers obtained by adding 20 mg (e), 40 mg (f), and 80 mg (g) of unimer (as a  $2 \text{ mg mL}^{-1}$  solution in hot MeCN) to 20 mg of seeds (Scale bars: 250 nm); h) Linear dependence of average contour length ( $L_n$ ) on the unimer to seed mass ratio. Reproduced from ref [24] with permission. Copyright 2015, Royal Society of Chemistry.

same experimental conditions as 1. After 4 weeks, the solution of 2 revealed a distinct new 2D platelet morphology alongside polydisperse fibers, whereas 3 showed the exclusive presence of 2D platelets after aging for 24 h (Figure 2). This phenomenon

manifests that the dynamic behavior changes by simple variations in the length of the solubilizing ancillary ligand and that this follows the expected trend based on packing parameters. The increase in dynamic behavior in the order  $1 < 2 < 3$  indicates the necessity for a long solubilizing ligand to suppress dynamic exchange.

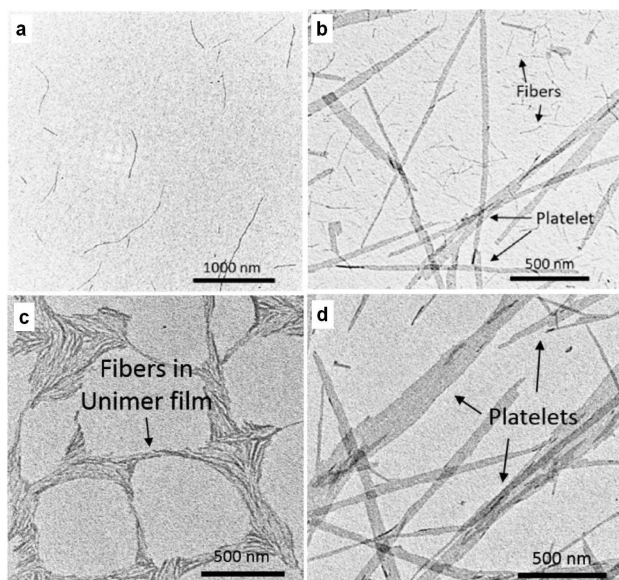


**Figure 2.** TEM micrographs of nanostructures of 2 obtained upon drop-casting a  $0.5 \text{ mg/mL}$  chloroform solution after being aged at  $21^\circ\text{C}$  for (a) 16 h and (b) 4 weeks; Platelet growth monitored by dissolving 3 at  $0.5 \text{ mg/mL}$  in chloroform at  $t = 0$  h (c) and  $t = 24$  h (d). Reproduced from ref [25] with permission. Copyright 2017, American Chemical Society.

## A.2. Pyridine bis-triazole ligands

The groups of De Cola and Strassert have extensively examined the self-assembly behavior of a variety of luminescent Pt(II) complexes.<sup>[23,26]</sup> In a ground-breaking example, De Cola, Mauro and coworkers reported a luminescent Pt(II) complex 4 based on a tridentate pyridine bis-triazole ligand (Figure 3a) and a glycol-appended pyridyl ancillary ligand that is able to form two distinct metastable aggregates (A and B) and a thermodynamically stable isoform C over time.<sup>[27]</sup> Injection of a 1,4-dioxane solution of monomeric 4 into water leads to metastable nanoparticle aggregates A *via* the isodesmic pathway. The hydrophobic Pt(II) fragments are efficiently shielded in the interior of the nanoparticles by the presence of peripheral OEG chains, leading to close intermolecular Pt(II)–Pt(II) interactions and red luminescence in the assembly. Over a period of three weeks, these nanoparticles transform into blue-emitting ribbon-like structures C, which represent the thermodynamically most stable assembly of 4. Solvent composition-dependent as well as variable temperature (VT)–UV/Vis and photoluminescence (PL) studies revealed a cooperative mechanism for the formation of

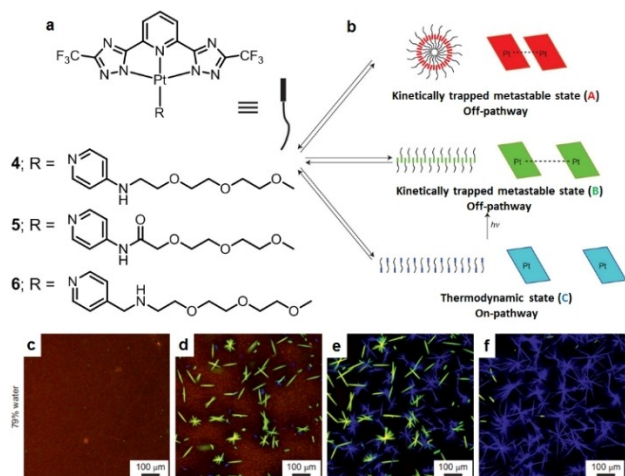


**Figure 3.** a) Chemical structure of Pt(II) complexes, 4–6; b) Schematic representation of the aggregates **A** (top), **B** (middle) and **C** (bottom) which are in dynamic equilibrium with the monomer. Right, the extent of Pt(II)–Pt(II) interactions for each assembly is shown graphically. The strength of the interactions decreases from **A** to **B**; no interaction is present in **C**. c–f) Time-dependent confocal microscopy of assembly of **4** in 79% water starting from **A** (red) into **B** (green) and finally **C** (blue),  $\lambda_{exc} = 405$  nm. Reproduced from ref [27] with permission. Copyright 2016, Macmillan Publishers Limited.

**C.** Surprisingly, during the transformation from **A** to **C**, another green luminescent metastable state (**B**) was found depending on the solvent composition, which was monitored by real-time fluorescence confocal microscopy (Figure 3c–f). Green fluorescence arises from an emitting metal-metal-to-ligand charge transfer (MMLCT) excited state as a consequence of Pt(II)–Pt(II) interactions with a slightly longer metal-metal distance than that in **A**. Ultimately, this species evolves to the thermodynamic aggregate **C** where no short Pt(II)–Pt(II) contacts are present. In analogy to the previous report by Manners, the authors also performed seed-induced LSP. However, in contrast to the example by Manners where the monomer solution was added to the seed solution, in the current example the seeds were prepared from thermodynamic aggregate **C** and added to pure metastable aggregate **A**.

In a more recent work,<sup>[28]</sup> the same group has shown how minor structural changes of the monomer units can affect both the kinetics and thermodynamics of the assemblies. To this end, the authors synthesized two new Pt(II) complexes **5** and **6** that differ from **4** in the nature of the linking group connecting the OEG chains to the pyridyl ligand (Figure 3a). Whereas for **5** the amine bond of **4** was replaced by an amide connectivity, an additional methylene groups was added in **6** to separate the amino group and the ancillary pyridyl ligand. In analogy to **4**, **5** also forms three different aggregates (**A**, **B** and **C**) depending on the solvent ratio. However, in sharp contrast to **4**, aggregate **C** is absent in the case of complex **6**, which highlights the crucial role of the linking group in determining the energy landscape of the system.

### A.3. Alkynyl terpyridine ligands

The groups of Yam, Eisenberg, and Tung have extensively explored alkynyl terpyridine-based tridentate ligands due to their rich photophysics, spectroscopic properties and multiple potential applications in molecular recognition, as pH sensors, biomolecular labels and so on.<sup>[29–31]</sup> In particular, Yam and coworkers have greatly contributed to understanding the self-assembly behavior and structure-property relationship of alkynylplatinum(II) terpyridine complexes that are assembled by Pt(II)–Pt(II) and  $\pi$ – $\pi$  stacking interactions.<sup>[29]</sup> In a recent example, they have reported the LSP of a system composed of two structurally dissimilar components: i) Pt(II) complexes (**7**, **8** and **9**; Figure 4a) and, ii) diblock copolymers, poly(ethylene glycol)-*b*-poly(acrylic acid) (PEG-*b*-PAA).<sup>[32]</sup> Such two-component LSP systems remain less investigated in comparison to the single-component-based ones, as shown for example in the previous section. The role of PAA blocks is to neutralize the charges of the Pt(II) complexes and direct the longitudinal growth into 1D crystalline nanostructures by noncovalent metal-metal and  $\pi$ – $\pi$  interactions, whereas the PEG blocks inhibit the transversal growth of the Pt(II) complexes. Supramolecular co-assembly of complex **7** and PEG<sub>45</sub>-*b*-PAA<sub>69</sub> in a solvent mixture of CH<sub>3</sub>CN:MeOH:H<sub>2</sub>O (1:1:8, v/v/v) instantly leads to nanoparticles which upon aging further transform into long fibers *via* a nucleation-growth mechanism (Figure 4b). In this case, the authors did not prepare seeds separately by sonication such as the previous reports by Manners and De Cola, as the ends of these long fibers remain active and act themselves as seeds. The authors performed LSP by adding the monomeric solution of complex **7** into two different co-assembled supramolecular polymers (complex **7** and PEG<sub>113</sub>-*b*-PAA<sub>51</sub> or complex **8** and PEG<sub>45</sub>-*b*-PAA<sub>69</sub>) separately. The increase in length of the nanofibers suggests the presence of active ends that serve as nucleation sites for the growth of the added complex **7** (Figure 4c–d). On the other hand, complex **9**, which features a larger  $\pi$ -surface, was found to form nanorods in water, which may serve as seeds for subsequent supramolecular growth. In fact, addition of a mixture of complex **7** and PEG<sub>45</sub>-*b*-PAA<sub>69</sub> to the nanorods of **9** induced the formation of 1D segmented nanostructures where nanofiber segments of complex **7** connect nanorod segments of complex **9** to form heterojunctions (Figure 4e–f).

In a separate work, the same group reported the pathway complexity in the supramolecular polymerization of two-component systems.<sup>[33]</sup> The core-shell nanofibers obtained from supramolecular co-assembly of complex **7** and PEG<sub>45</sub>-*b*-PAA<sub>69</sub> in a mixed solvent is a kinetically trapped state, as it allows only longitudinal growth upon incubation at room temperature. On the other hand, thermal annealing can switch on the transversal growth of Pt(II) complexes and block copolymers into thermodynamically stable core-shell nanobelts, where the extent of transversal growth increases with thermal annealing temperatures. Upon rapid thermal quenching, the mixture of complex **7** and PEG<sub>45</sub>-*b*-PAA<sub>69</sub> was found to form nanobelt-*b*-nanofiber nanostructures (Figure 5b–c), where the nanobelt segment connects several nanofiber segments in an end-to-end manner.

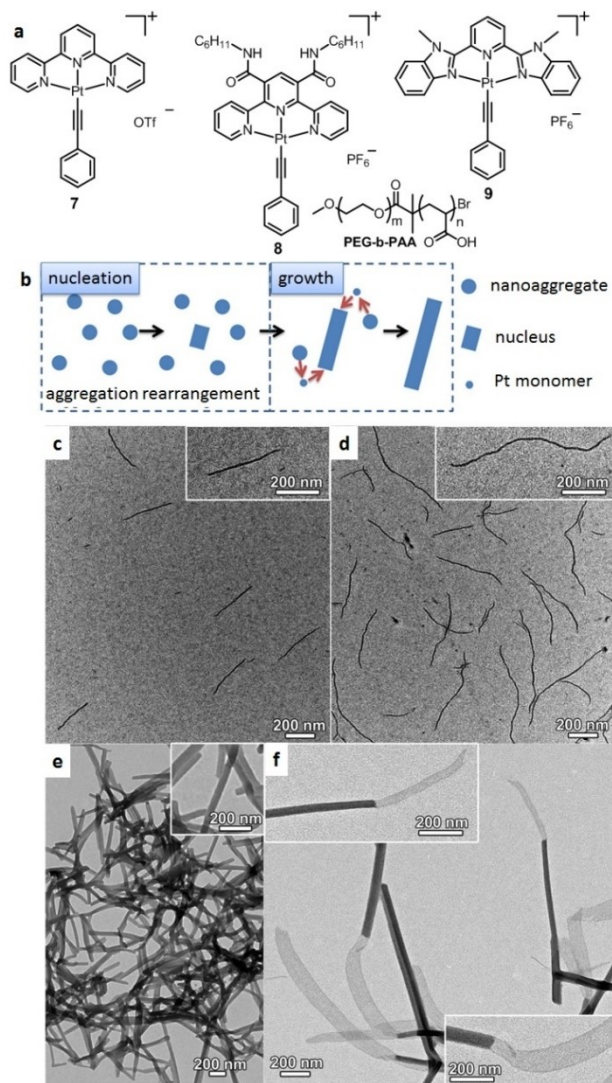


**Figure 4.** a) Chemical structure of Pt(II) complexes 7–9; b) Pictorial representation of the supramolecular co-assembly by the nucleation-growth mechanism; TEM images of c) nanofibers formed by supramolecular co-assembly of **7** (0.06 mM) and PEG<sub>113</sub>-*b*-PAA<sub>51</sub> ([carboxylic acid] = 1.2 mM) in a mixed solvent of CH<sub>3</sub>CN:MeOH:H<sub>2</sub>O (1:1:8); d) longer nanofibers formed after adding more **7** to the as-formed nanofibers of (c) at a final **7**/carboxylic acid molar ratio of 0.1/1; e) nanorods formed by supramolecular coassembly of **8** (0.11 mM) and PEG<sub>45</sub>-*b*-PAA<sub>69</sub> ([carboxylic acid] = 1 mM) in the same solvent mixture; f) segmented nanostructures formed after adding **7** to the as-formed nanorods of (e) at a final **7**/**8**/carboxylic acid molar ratio of 0.18/0.11/1. Reproduced from ref [32] with permission. Copyright 2017, United States National Academy of Science.

These results suggest that the nanobelt segments are formed in the initial stages of the cooling process, when the temperature is higher than room temperature. Upon cooling the mixture of complex **7** and PEG<sub>45</sub>-*b*-PAA<sub>69</sub> to room temperature, nanobelt segments would act as seeds to initiate the subsequent self-assembly processes resulting in nanobelt-*b*-nanofiber nanostructures. The core-shell nanofibers (Figure 5d) obtained from the mixture can be broken into patchy nanofibers (Figure 5e) upon sonication at 0 °C for 1 h. After incubation, these patchy nanofibers further transformed into 2D core-shell nanobelts (Figure 5f).<sup>[34]</sup>

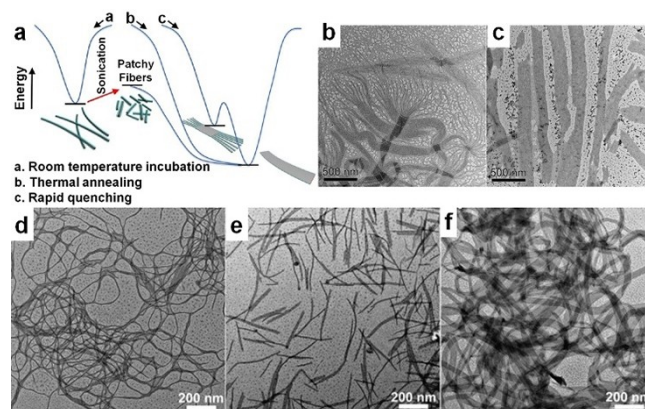


**Figure 5.** a) Energy profile diagram of the nanobelt-*b*-nanofiber nanostructures and their subsequent fusion into nanobelts; TEM images of the b) nanobelt-*b*-nanofiber nanostructures captured by rapid quenching of the mixture of complex **7** (0.15 mM) and PEG<sub>45</sub>-*b*-PAA<sub>69</sub> ([carboxylic acid] = 1 mM) in a solvent mixture of CH<sub>3</sub>CN:MeOH:H<sub>2</sub>O (1:1:8) (heating to 70 °C, fast cooling to rt); c) nanobelts formed by rt incubation of the nanobelt-*b*-nanofiber nanostructures for 1 week. Reproduced with permission from ref [33]. Copyright 2018, American Chemical Society. TEM images of d) the core-shell nanofibers prepared from **7** and PEG<sub>45</sub>-*b*-PAA<sub>69</sub> in a mixed solvent of CH<sub>3</sub>CN:MeOH:H<sub>2</sub>O (1:2:7); e) patchy nanofibers formed by sonication of the core-shell nanofibers in (d) at 0 °C for 1 h, and (e) nanobelts formed by incubation of the patchy nanofibers in (f). Reproduced with permission from ref [34]. Copyright 2017, Elsevier.

#### A.4. Tridentate cyclometalating ligands

Cyclometalating ligands of different kind such as N<sup>^</sup>C<sup>^</sup>N and C<sup>^</sup>N<sup>^</sup>N are typically used as tridentate ligands in metal coordination.<sup>[35]</sup> Particularly, cyclometalated d<sup>8</sup> metal complexes have gained increasing attention due to their enhanced emission properties in comparison to terpyridine systems due to stronger  $\sigma$ -donation ability. The groups of Yam, Che, Wang and others have investigated the photophysical properties of different Pt(II) complexes based on cyclometalating ligands. In analogy to previously described tridentate-based systems, Che and co-workers have recently demonstrated that cyclometalated Pd(II) complexes are also able to undergo competing supramolecular processes and LSP. In their example, the authors designed and investigated three mononuclear cyclometalated Pd(II) complexes based on (C<sup>^</sup>N<sup>^</sup>N) ligands (**10a**, **10b** and **10c**; Figure 6a) that only differ from one another in their counteranions (PF<sub>6</sub><sup>-</sup>, OTf<sup>-</sup>, ClO<sub>4</sub><sup>-</sup>).<sup>[36]</sup> This structural difference is expected to influence the cation-anion electrostatic and cation-cation dispersive interactions and, subsequently, the self-assembly behaviour. Supramolecular polymerization of **10a** (PF<sub>6</sub><sup>-</sup>) initially undergoes a disfavored nucleation step followed by a highly favored elongation process, whereas **10b** (OTf<sup>-</sup>) follows the isodesmic mechanism for the oligomerization. These results clearly highlight the strong influence caused by the counteranion on the self-assembly mechanism. Upon injecting H<sub>2</sub>O into an acetonitrile solution of **10a**, a kinetically trapped aggregate (Agg<sub>1</sub>) is formed instantly, which over a lag time transforms into a second aggregate species (Agg<sub>2</sub>). This is illustrated in the energy landscape of Figure 6. Interestingly, this aggregate Agg<sub>2</sub> exhibits a preferential 1D growth with close

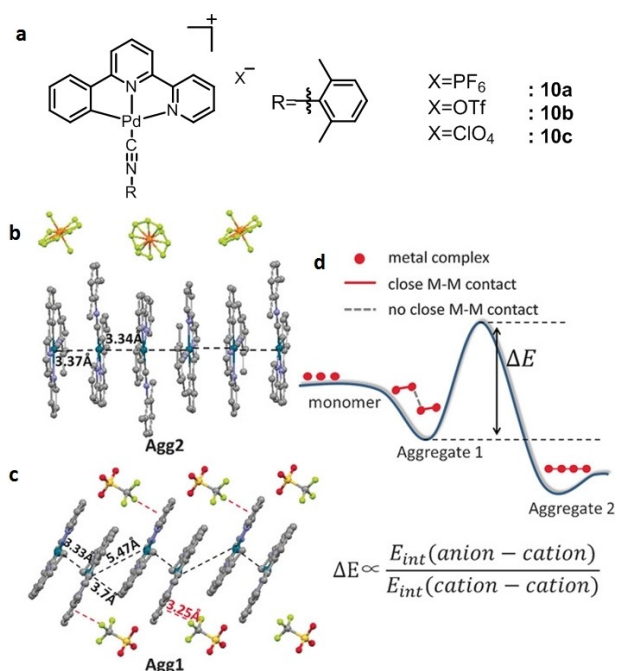


**Figure 6.** a) Chemical structures of Pd(II) complexes **10a–c**; b) Crystal structure of **10a** featuring a 1D infinite structure with a Pd(II)–Pd(II) chain; c) Crystal structure of **10b** highlighting the cation pair features, Hydrogen atoms are omitted for clarity. d) Qualitative energy landscape of supramolecular polymerization models with a competing kinetic stabilization state. Reproduced from ref [36] with permission. Copyright 2018, Wiley VCH.

Pd(II)–Pd(II) contacts, as evident from crystal structure analysis (Figure 6b). In contrast, the OTf<sup>−</sup> counterion of **10b** has a key impact on both the molecular packing and the ability of the system to exhibit pathway complexity.

As shown in the crystal structure of **10b** (Figure 6c), the counteranions OTf<sup>−</sup> establish close contacts with the pyridyl ring of the Pd(II) complex, thereby preventing short Pd(II)–Pd(II) contacts between neighbouring cation pairs. As a result, 1D growth is inhibited and aggregation is stopped at Agg<sub>1</sub> state. Finally, **10c** with counteranion ClO<sub>4</sub><sup>−</sup> also forms initially the Agg<sub>1</sub> state, but however the conversion to the thermodynamic state Agg<sub>2</sub> is very slow. Intriguingly, this transformation can be accelerated without any lag phase upon addition of seeds obtained from Agg<sub>2</sub> of **10a**. In contrast to the previously described examples from Manners, De Cola and Yam, in the present manuscript, Che and co-workers have used a dilution method in order to prepare the seeds. Thus, this elegant example highlights the strong influence exerted by counterions on the kinetic vs. thermodynamic pathways of metal-containing self-assembled systems. In another work,<sup>[37]</sup> the same group has shown a related phenomenon for the chiral Pt(II) complexes **11a**, **11b** and **11c** (Figure 7a) using the same counteranions as the previous report. Among them, **11a** and **11b** with counteranions PF<sub>6</sub><sup>−</sup> and OTf<sup>−</sup> respectively, can form stable aggregates. The CD spectrum of **11a** in a monomeric state shows a weak CD signal which is greatly enhanced upon aggregation but in case of **11b**, the CD signal remains weak in the aggregated state even after several days. In contrast, complex **11c** with

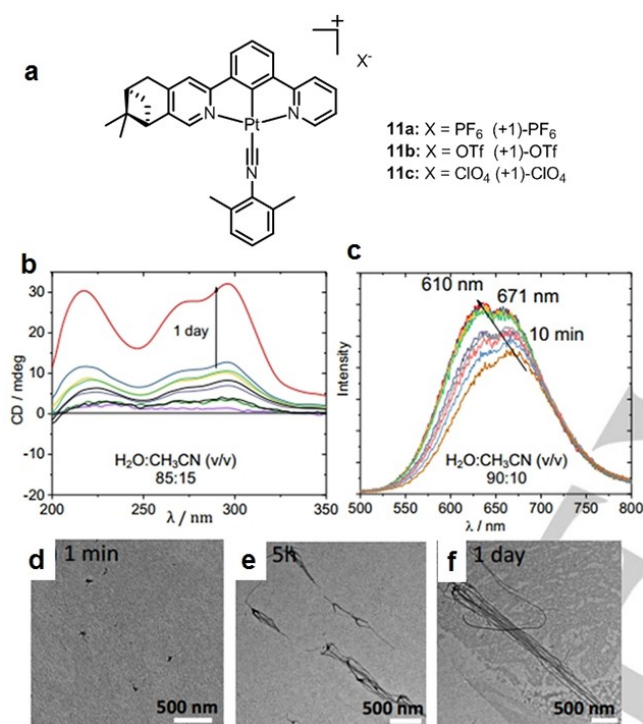


**Figure 7.** a) Chemical structures of the Pt(II) complexes **11a–c**; b) time-dependent CD spectra, c) emission spectra, TEM images d–f, H<sub>2</sub>O/CH<sub>3</sub>CN = 85:15 v/v of **11c** (1.0 × 10<sup>−4</sup> M). Reproduced from ref [37] with permission. Copyright 2018, Wiley VCH.

ClO<sub>4</sub><sup>−</sup> forms kinetically trapped metastable weak emissive nanoparticles at the initial stage with an insignificant CD signal, similar to **11b**. Over time, these nanoparticles elongate to thermodynamically stable nanowires with enhanced emission and pronounced CD signals (Figure 7b–f). LSP of **11c** has been performed up to three cycles by applying seeds made of **11a** and monitored by CD spectroscopy and TEM.

In addition to Pd(II) and Pt(II) complexes, assemblies of their isoelectronic d<sup>8</sup> Au(III) analogs have also been explored,<sup>[21b]</sup> although to a much lower extent compared to the former. This can be explained by their comparatively lower stability and emission properties in solution as a result of low-lying d–d ligand field excited states of Au(III).<sup>[38]</sup> Very recently, the groups of Yam and Che have made important contributions to the development of various d<sup>8</sup> Au(III) complexes based on tridentate and tetradentate ligands that can self-assemble *via* Au(III)–Au(III) and π–π interactions.<sup>[39]</sup> In analogy to previously described pathway complexity of Pt(II) and Pd(II) complexes, Che and co-workers have demonstrated that Au(III) complexes are also able to undergo kinetically controlled self-assembly and LSP. In this work, pincer type Au(III) complexes with different counteranions (PF<sub>6</sub><sup>−</sup>, ClO<sub>4</sub><sup>−</sup>, OTf<sup>−</sup>) were synthesized and investigated (**12a**, **12b** and **12c**, respectively, Figure 8).<sup>[40]</sup> It could be shown that the counteranions also play a key role in dictating the self-assembly behavior, in a similar manner as for the previously described, structurally related Pd(II) and Pt(II) complexes **10** and **11** reported by the same group. Kinetic studies of **12a** and **12b** in H<sub>2</sub>O/CH<sub>3</sub>CN (9/1) mixtures reveal that

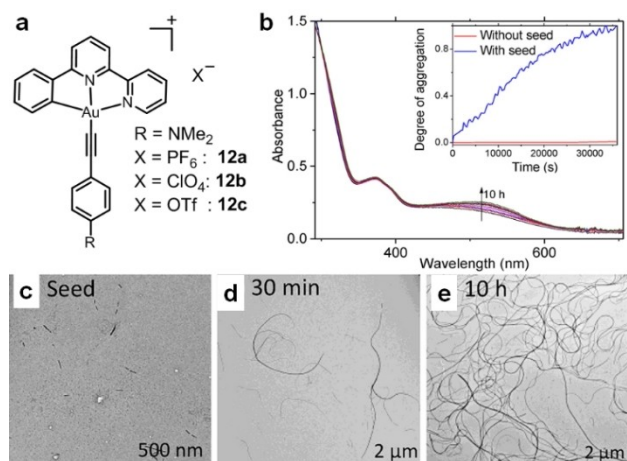


**Figure 8.** a) Molecular structures of Au(III) complexes, **12a-c**; b) Time-dependent UV-vis absorption spectra of **12b** after addition of seeds prepared from **12a** ( $c = 5 \times 10^{-5}$  M for **12b** and  $2 \times 10^{-5}$  M for seed **12a**). Inset: Time-dependent degree of aggregation calculated at 530 nm for **12b** with and without the seeds. c) TEM image of the seeds; Time-dependent TEM images of **12b** with the seeds obtained at d) 30 min and e) 10 h, respectively. Reproduced with permission from ref [40]. Copyright 2019, American Chemical Society.

both the complexes followed a kinetically controlled supramolecular polymerization process but under the same condition **12c** does not show such a behavior. The lag phase for **12b** is longer than that for **12a**, suggesting that the energy barrier between the kinetic and thermodynamic product is higher for **12b** than for **12a**. This high kinetic barrier slows down the transformation rate from kinetic to thermodynamic state in the case of **12b** due to strong interactions between the  $\text{ClO}_4^-$  counterions and the cationic complex. To accelerate this transformation, the authors have performed seed-induced LSP and monitored this process by UV/Vis and TEM (Figure 8). The seeds were prepared from the thermodynamic state of **12a** by dilution as before and added to the solution of **12b** in  $\text{CH}_3\text{CN}$ . After addition of seeds, the lag phase disappeared, and time-dependent TEM images revealed the growth of nanofibers. The counteranion,  $\text{PF}_6^-$  from **12a** seeds actually assists to break the Au(III) complex- $\text{ClO}_4^-$  interaction in **12b** and facilitates the transition to the thermodynamic state.

## B. Monodentate ligands

Although the self-assembly features and pathway complexity of  $d^8$  complexes with tridentate ligands are relatively well understood, their counterparts featuring monodentate ligands such as pyridyl groups have remained comparatively less explored. These systems have been primarily investigated in terms of their liquid crystalline behavior or gelation ability rather than in solution.<sup>[41-42]</sup> In the previous sections, we have seen that the high planarity of the  $d^8$  metal center imposed by the use of chelating tridentate ligands enables efficient aromatic and short meta-metal contacts. This situation is, however, rather different for  $d^8$  metal complexes based on monodentate ligands, as the

larger number of coordinating ligands dramatically affects the planarity and sterics of the metal center. However, at the same time, these inherent geometrical considerations confer such systems a unique property: various possibilities of molecular arrangements during aggregation, which is a prerequisite to achieve pathway complexity. This particularly applies to those systems with balanced repulsive and attractive interactions, for example  $d^8$  *trans*-complexes with two bulky ligands and two highly preorganized ligands with a large aromatic surface. Typical systems that fulfill these requirements are *trans*-Pt(II) and Pd(II) complexes containing two chlorido ligands and two pyridyl ligands featuring an extended aromatic surface derived from oligophenyleneethynylene (OPE), which have been widely investigated by our group.<sup>[43]</sup> Comprehensive studies supported by theoretical calculations have enabled us to gain insights into the packing modes, nanoscale morphology and self-assembly mechanism of these systems, particularly from a thermodynamic point of view. Based on our results, we can conclude that both the nature of the metal ion (Pd(II) or Pt(II)), and the polarity and volume of the side chains play a key role in the assembly stabilization, which can occur through a wide range of weak non-covalent forces. Early studies for some of these complexes focused on the thermodynamic aspects of the supramolecular polymerization. However, in analogy to other systems in the literature, subtle modulation of various experimental conditions (solvent, temperature, concentration, cooling rate, sonication) enables the emergence of competing kinetic paths. An illustrative case is exemplified by a hydrophobic bispyridyldichlorido Pt(II) complex **13**, which comprises an extended OPE-based aromatic surface, amide groups and peripheral alkoxy chains (Figure 9). Depending on the cooling rate and concentration, **13** self-assembles in methylcyclohexane (MCH) into two highly stable competing supramolecular polymorphs (**A** and **B**) with distinct molecular packing (slipped vs. pseudo-parallel, respectively).<sup>[44]</sup> The formation of two distinct supramolecular polymers was monitored by VT UV/Vis spectroscopy (Figure 9b-d). The polymorph **A** is preferentially obtained upon cooling hot monomer solutions of **13** at relatively fast cooling rates of  $2 \text{ K min}^{-1}$ . This aggregate is formed *via* an isodesmic mechanism and stabilized by aromatic as well as unconventional  $\text{N-H}\cdots\text{Cl-Pt}$  interactions. This results in an absorption spectrum that is red-shifted with respect to the monomer absorption (Figure 9b). On the other hand, slow cooling using rates of  $0.1 \text{ K min}^{-1}$  primarily leads to the formation of a different aggregate species (polymorph **B**), which is characterized spectroscopically by a decrease in absorption yet no significant shifts compared to the monomer species (Figure 9d). In contrast to **A**, this cooperative assembly is stabilized by  $\text{N-H}\cdots\text{O-alkoxy}$  hydrogen bonding as well as aromatic interactions of pseudoparallel-arranged molecules, as shown in Figure 9a. Interestingly, under intermediate cooling rates ( $0.5 \text{ K min}^{-1}$ ), both polymorphs coexist without interconversion even after several months, which demonstrates the minor energy difference between the two species (around  $4 \text{ kJ mol}^{-1}$ ). The transformation of **A** to **B** *via* monomer could only take place upon thermal annealing of kinetic species **A** at elevated temperatures. The stability of both species is eluci-



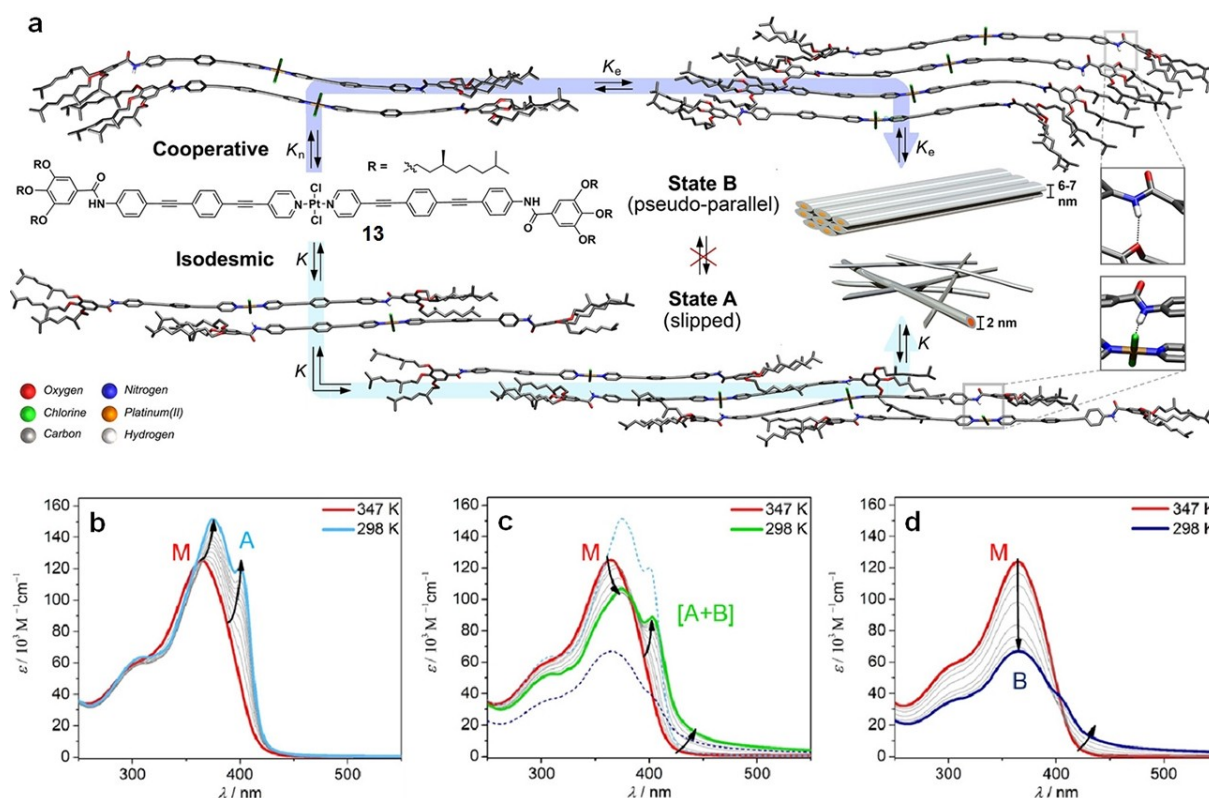


**Figure 9.** a) Chemical structure of 13 and dispersion-corrected PM6 calculations depicting its concomitant supramolecular polymerization; b–d) Variable-temperature UV–vis experiments of 13 in MCH at 100  $\mu\text{M}$  between 347 K and 298 K, with a cooling rate of (b) 2  $\text{K min}^{-1}$ , (c) 0.5  $\text{K min}^{-1}$ , and (d) 0.1  $\text{K min}^{-1}$ . The red spectra correspond to the monomer species, which converts into aggregate type A (cyan), type B (royal blue), or a mixture of A and B (green) on cooling. Reproduced from ref [44] with permission. Copyright 2019, American Chemical Society.

dated by precise control of temperature, concentration and cooling rate, which was represented through a phase diagram. Distinct structural differences of different species can also be monitored by atomic force microscopy (AFM), where thin flexible fibers were visualized for species A in sharp contrast to significantly longer, more rigid, and thicker fibers for species B.

In a recent example, we have demonstrated a novel way to control competing anti-cooperative vs. cooperative aggregation pathways by introducing chain immiscibility in our molecular design. For this purpose, we designed a linear OPE-based amphiphilic Pt(II) complex 14 that is unsymmetrically substituted with triethyleneglycol (TEG) and dodecyloxy side chains (Figure 10a).<sup>[45]</sup> This molecular design is responsible for the creation of two distinct yet stable aggregates that follow two different mechanisms: kinetically controlled anticooperative nanoparticle assemblies (A) and thermodynamically controlled cooperative supramolecular polymers (B) (Figure 10b). Intriguingly, the absorption changes in MCH upon cooling a monomer solution from 353 K to 280 K revealed two clearly defined regimes that can be assigned to the formation of two aggregate species with distinct stability. Cooling to intermediate temperatures (303 K) leads to an anticooperative assembly A with weak  $\pi$ -coupling (green plot in Figure 11a). Further cooling the same solution to 283 K leads to a cooperative assembly B that is characterized by a red-shifted aggregate spectrum compared to the monomer species at 353 K (see red and blue plots in

Figure 11a). This spectral pattern is typical for slipped  $\pi$ -stacks, as supported by NMR studies. The presence of two regimes in the aggregation of 14 is supported by the two-step plots obtained in cooling experiments (inset of Figure 11a) or in solvent-dependent denaturation studies (where the aggregates in MCH are disassembled by adding  $\text{CHCl}_3$ , Figure 11b). Detailed analysis at multiple concentrations ultimately enabled the derivation of experimental phase diagrams revealing the stability conditions of the three species (M, A, and B) present in equilibrium (Figure 11c).

## Conclusion and outlook

Supramolecular polymerization of metal complexes has been a hot topic of research in the last decade because of the versatility of applications provided by the metal ions. Among these,  $d^8$  metal complexes, primarily Pt(II) complexes, have been extensively explored due to their outstanding photophysical and supramolecular properties stemming from the presence of aromatic and metal-metal interactions. Whereas the majority of early examples of  $d^8$ -based supramolecular polymers have been assumed to operate under thermodynamic control, more recent detailed experimental studies and sophisticated sample preparation protocols have allowed to identify competing kinetically controlled processes. In this minireview, we have collected

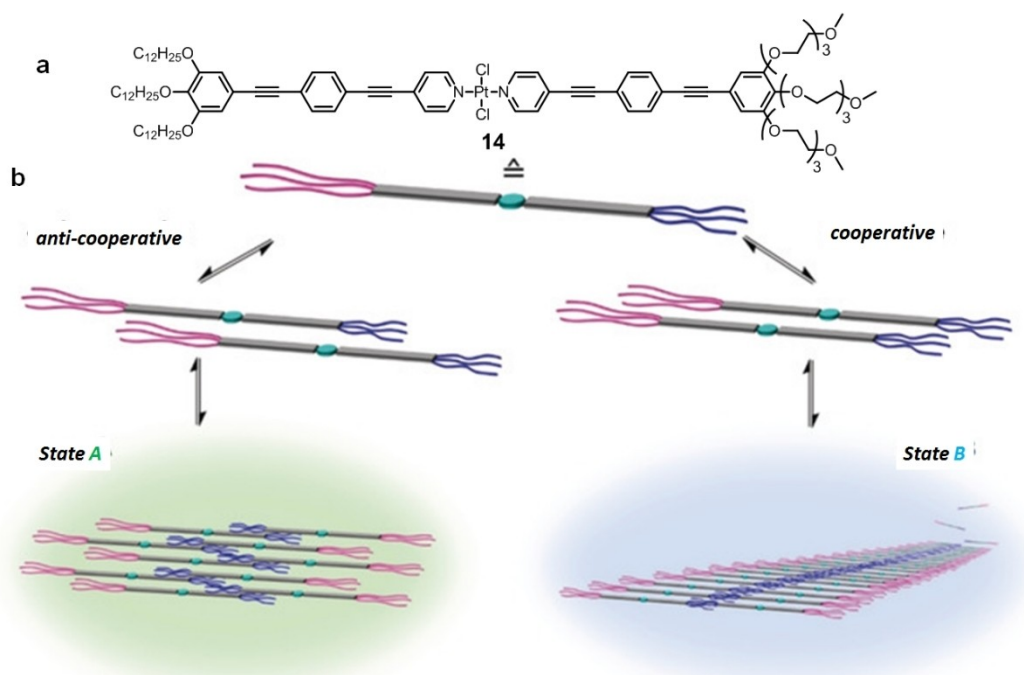


**Figure 10.** a) Chemical structure of **14**; b) schematic depiction of the self-assembly pathways leading to aggregate species **A** and **B**. Reproduced from ref [45] with permission. Copyright 2019, Wiley VCH.

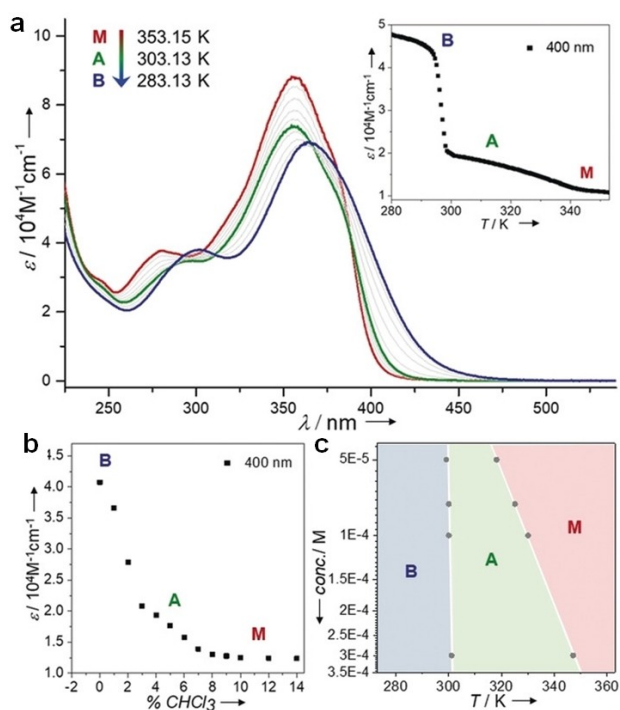


**Figure 11.** a) Temperature-dependent UV/Vis spectra of **14** at  $3 \times 10^{-4}$  M in MCH from 353 K to 283 K at a cooling rate of  $0.2 \text{ K min}^{-1}$ . Inset: Plot of the extinction coefficient ( $\lambda = 400 \text{ nm}$ ) as a function of temperature. b) Plot of the extinction coefficient ( $\lambda = 400 \text{ nm}$ ) as a function of the volume percentage of  $\text{CHCl}_3$  in MCH ( $c = 3 \times 10^{-4} \text{ M}$ ) at 298 K. c) Experimental phase diagram showing the stability conditions of the monomer, species **A**, and species **B** in MCH. Reproduced from ref [45] with permission. Copyright 2019, Wiley VCH.

recent examples of  $d^8$  metal complexes that can undergo competing thermodynamic vs. kinetic polymerization pathways in a controlled fashion. Pathway control in these systems can be achieved by careful selection of various experimental conditions (solvent composition, temperature, concentration, etc.) as well as by molecular design. Particularly, control over the kinetics in these systems has allowed to tune the supramolecular polymer length *via* a seeded-growth approach. The majority of assemblies of  $d^8$  metal complexes include chelating tridentate ligands in the molecular design, which enable strong aromatic and metal-metal interactions due to a planar, accessible geometry of the metal center. For these systems, pathway complexity (and LSP) has been primarily achieved in aqueous media, suggesting that strong hydrophobic forces and slow dynamics in water<sup>[46]</sup> represent an important driving force for the identification of kinetically controlled pathways. On the other hand,  $d^8$  metal complexes based on monodentate pyridyl ligands have been shown to exhibit pathway complexity in both polar and nonpolar media, being the kinetic stability of some of these aggregates remarkably high. This behaviour probably results from the lower preorganization and increased sterics of the metal center compared to tridentate-based systems. As a result, the stronger competition between attractive and repulsive interactions makes the formation of different aggregates of close energy more probable. On this basis, we believe that the stabilization of kinetic products formed by tridentate-based systems can be achieved by slightly disturbing their highly planar surface by introducing minor bulkiness in the molecular design. Additionally, other strategies such as the fine-tuning of counterions, chain immiscibility,

variations in the length of the  $\pi$ -surface or solubilizing groups and the inclusion of hydrogen bonding groups are expected to control the structural, morphological, and spectroscopic properties of the  $d^8$  metal complexes and their self-assemblies. The robustness of the metal-ligand bonds and the stability of the complexes are also important factors to consider. This may be one of the reasons why the investigation of competing pathways of more labile  $d^8$  Ni(II) complexes, which are isoelectronic with Pt(II), Pd(II) and Au(III), has remained unexplored. The fundamental understanding extracted from the recent studies reported in this review is expected to pave the way to sophisticated metallosupramolecular luminescent functional materials with tunable size and shape. The tunability of metallosupramolecular assembly can play an important role to determine not only the charge transport and optical properties of materials, such as organic light emitting diodes (OLEDs) and organic memory devices, but also biomolecules and enzymatic activities for early diagnosis of various diseases. We believe that this may bring new opportunities for supramolecular chemists to expand the field by molecular design of new ligands as well as other  $d^8$  metal centers.

## Acknowledgements

G.G. and G.F. thank the European Commission for funding (ERC-StG-2016 SUPRACOP-715923). T.G. thanks the University of Münster for a WWU fellowship.

## Conflict of Interest

The authors declare no conflict of interest.

**Keywords:**  $d^8$  metal complexes · pathway complexity ·  $\pi$ -conjugated systems · self-assembly · supramolecular polymerization

- [1] a) T. F. A. de Greef, M. M. J. Smulders, M. Wolffs, A. P. H. J. Schenning, R. P. Sijbesma, E. W. Meijer, *Chem. Rev.* **2009**, *109*, 5687–5754; b) A. Mishra, C.-Q. Ma, P. Bäuerle, *Chem. Rev.* **2009**, *109*, 1141–1276; c) T. Aida, E. W. Meijer, S. I. Stupp, *Science* **2012**, *335*, 813–817; d) L. Maggini, D. Bonifazi, *Chem. Soc. Rev.* **2012**, *41*, 211–241; e) S. S. Babu, V. K. Praveen, A. Ajayaghosh, *Chem. Rev.* **2014**, *114*, 1973–2129; f) C. Rest, R. Kandaneli, G. Fernández, *Chem. Soc. Rev.* **2015**, *44*, 2543–2572; g) F. Würthner, C. R. Saha-Möller, B. Fimmel, S. Ogi, P. Leowanawat, D. Schmidt, *Chem. Rev.* **2016**, *116*, 962–1052.
- [2] a) S. I. Stupp, *Nano Lett.* **2010**, *10*, 4783–4786; b) J. D. Tovar, *Acc. Chem. Res.* **2013**, *46*, 1527–1537; c) B. O. Okesola, Y. Wu, B. Derkus, S. Gani, D. Wu, D. Knani, D. K. Smith, D. J. Adams, A. Mata, *Chem. Mater.* **2019**, *31*, 7883–7897.
- [3] M. M. Bouman, E. W. Meijer, *Adv. Mater.* **1995**, *7*, 385–387.
- [4] P. Jonkheijm, P. van der Schoot, A. P. H. J. Schenning, E. W. Meijer, *Science* **2006**, *80*, 80–83.
- [5] P. A. Korevaar, S. J. George, A. J. Markvoort, M. M. J. Smulders, P. A. J. Hilbers, A. P. H. J. Schenning, T. F. A. de Greef, E. W. Meijer, *Nature* **2012**, *481*, 492–496.
- [6] S. Ogi, K. Sugiyasu, S. Manna, S. Samitsu, M. Takeuchi, *Nat. Chem.* **2014**, *6*, 188–195.
- [7] a) J. Kang, D. Miyajima, T. Mori, Y. Inoue, Y. Itoh, T. Aida, *Science* **2015**, *347*, 646–651; b) S. Ogi, V. Stepanenko, K. Sugiyasu, M. Takeuchi, F. Würthner, *J. Am. Chem. Soc.* **2015**, *137*, 3300–3307; c) D. S. Pal, H. Kar, S. Ghosh, *Chem. Commun.* **2018**, *54*, 928–931; d) E. E. Greciano, B. Matarranz, L. Sánchez, *Angew. Chem. Int. Ed.* **2018**, *57*, 4697–4701; *Angew. Chem.* **2018**, *130*, 4787–4791; e) S. Ogi, K. Matsumoto, S. Yamaguchi, *Angew. Chem. Int. Ed.* **2018**, *57*, 2339–2343; *Angew. Chem.* **2018**, *130*, 2363–2367; f) J. S. Valera, R. Gómez, L. Sánchez, *Small* **2018**, *14*, 1702437; g) A. Chakraborty, G. Ghosh, D. S. Pal, S. Varghese, S. Ghosh, *Chem. Sci.* **2019**, *10*, 7345–7351.
- [8] a) P. A. Korevaar, C. Schaefer, T. F. A. de Greef, E. W. Meijer, *J. Am. Chem. Soc.* **2012**, *134*, 13482–13491; b) P. A. Korevaar, C. J. Newcomb, E. W. Meijer, S. I. Stupp, *J. Am. Chem. Soc.* **2014**, *136*, 8540–8543.
- [9] a) T. Yamamoto, T. Fukushima, Y. Yamamoto, A. Kosaka, W. Jin, N. Ishii, T. Aida, *J. Am. Chem. Soc.* **2006**, *128*, 14337–14340; b) Y. Tidhar, H. Weissman, S. G. Wolf, A. Gulino, B. Rybtchinski, *Chem. Eur. J.* **2011**, *17*, 6068–6075; c) A. T. Haedler, S. C. J. Meskers, R. H. Zha, M. Kivala, H. Schmidt, E. W. Meijer, *J. Am. Chem. Soc.* **2016**, *138*, 10539–10545; d) Z. Chen, Y. Liu, W. Wagner, V. Stepanenko, X. Ren, S. Ogi, F. Würthner, *Angew. Chem. Int. Ed.* **2017**, *56*, 5729–5733; *Angew. Chem.* **2017**, *129*, 5823–5827.
- [10] a) H. Kar, G. Ghosh, S. Ghosh, *Chem. Eur. J.* **2017**, *23*, 10536–10542; b) G. Ghosh, S. Ghosh, *Chem. Commun.* **2018**, *54*, 5720–5723.
- [11] a) N. Micali, H. Engelkamp, P. G. van Rhee, P. C. M. Christianen, L. M. Scolaro, J. C. Maan, *Nat. Chem.* **2012**, *4*, 201–207; b) S. Yagai, S. Okamura, Y. Nakano, M. Yamauchi, K. Kishikawa, T. Karatsu, A. Kitamura, A. Ueno, D. Kuzuhara, H. Yamada, T. Seki, H. Ito, *Nat. Commun.* **2014**, *5*, 4013; c) M. Endo, T. Fukui, S. H. Jung, S. Yagai, M. Takeuchi, K. Sugiyasu, *J. Am. Chem. Soc.* **2016**, *138*, 14347–14353.
- [12] a) S. Ogi, T. Fukui, M. L. Jue, M. Takeuchi, K. Sugiyasu, *Angew. Chem. Int. Ed.* **2014**, *53*, 14363–14367; *Angew. Chem.* **2014**, *126*, 14591–14595; b) T. Fukui, S. Kawai, S. Fujinuma, Y. Matsushita, T. Yasuda, T. Sakurai, S. Seki, M. Takeuchi, K. Sugiyasu, *Nat. Chem.* **2017**, *9*, 493–499.
- [13] D. S. Pal, S. Ghosh, *Chem. Eur. J.* **2018**, *24*, 8519–8523.
- [14] M. Wehner, F. Würthner, *Nat. Rev. Chem.* **2020**, *4*, 38–53.
- [15] M. Hartlieb, D. H. Mans, S. Perrier, *Polym. Chem.* **2020**, *11*, 1083–1110.
- [16] J. Matern, Y. Dorca, L. Sánchez, G. Fernández, *Angew. Chem. Int. Ed.* **2019**, *58*, 16730–16740.
- [17] P. A. Korevaar, T. F. A. de Greef, E. W. Meijer, *Chem. Mater.* **2014**, *26*, 576–586.
- [18] A. Sorrenti, J. Leira-Iglesias, A. J. Markvoort, T. F. A. de Greef, T. M. Hermans, *Chem. Soc. Rev.* **2017**, *46*, 5476–5490.
- [19] H. Amouri, C. Desmarets, J. Moussa, *Chem. Rev.* **2012**, *112*, 2015–2041.
- [20] V. W.-W. Yam, K. M. Wong, *Chem. Commun.* **2011**, *47*, 11579–11592.
- [21] a) G. R. Whittell, M. D. Hager, U. S. Schubert, I. Manners, *Nat. Mater.* **2011**, *10*, 176–188; b) V. W.-W. Yam, V. K.-M. Au, S. Y.-L. Leung, *Chem. Rev.* **2015**, *115*, 7589–7728; c) P. Wang, H. Wang, Y. Fang, H. Li, J.-H. He, Y. Ji, Y. Li, Q.-F. Xu, J. Zheng, J.-M. Lu, *ACS Appl. Mater. Interfaces* **2017**, *9*, 32930–32938; d) S. Sinn, F. Biedermann, L. De Cola, *Chem. Eur. J.* **2017**, *23*, 1965–1971; e) A. Ahmedova, *Front. Chem.* **2018**, *6*, 1–20; f) L. N. Neumann, C. Calvino, Y. C. Simon, S. Schrettl, C. Weder, *Dalton Trans.* **2018**, *47*, 14184–14188; g) J. B. Arockiam, H. Son, S. H. Han, G. Balamurugan, Y. Kim, J. S. Park, *ACS Appl. Energy Mater.* **2019**, *2*, 8416–8424.
- [22] K. M.-C. Wong, V. W.-W. Yam, *Acc. Chem. Res.* **2011**, *44*, 424–434.
- [23] M. Mauro, A. Aliprandi, D. Septiadi, N. S. Kehr, L. De Cola, *Chem. Soc. Rev.* **2014**, *43*, 4144–4166.
- [24] M. E. Robinson, D. J. Lunn, A. Nazemi, G. R. Whittell, L. De Cola, I. Manners, *Chem. Commun.* **2015**, *51*, 15921–15924.
- [25] M. E. Robinson, A. Nazemi, D. J. Lunn, D. W. Hayward, C. E. Boott, M.-S. Hsiao, R. L. Harniman, S. A. Davis, G. R. Whittell, R. M. Richardson, L. De Cola, I. Manners, *ACS Nano* **2017**, *11*, 9162–9175.
- [26] a) C. A. Strassert, C.-H. Chien, M. D. G. Lopez, D. Kourkoulos, D. Hertel, K. Meerholz, L. De Cola, *Angew. Chem. Int. Ed.* **2011**, *50*, 946–950; *Angew. Chem.* **2011**, *123*, 976–980; b) A. Galstyan, A. R. Naziruddin, C. Cebrián, A. Iordache, C. G. Daniliuc, L. De Cola, C. A. Strassert, *Eur. J. Inorg. Chem.* **2015**, 5822–5831; c) S. Carrara, A. Aliprandi, C. Hogan, L. De Cola, *J. Am. Chem. Soc.* **2017**, *139*, 14605–14610; d) Y. Atoini, E. A. Prasetyanto, P. Chen, S. Silvestrini, J. Harrowfield, L. De Cola, *Chem. Eur. J.* **2018**, *24*, 12054–12060; e) S. Sinn, L. Yang, F. Biedermann, D. Wang, C. Kübel, J. J. L. M. Cornelissen, L. De Cola, *J. Am. Chem. Soc.* **2018**, *140*, 2355–2362.
- [27] A. Aliprandi, M. Mauro, L. De Cola, *Nat. Chem.* **2016**, *8*, 10–15.
- [28] A. Aliprandi, L. Capaldo, C. Bobica, S. Silvestrini, L. De Cola, *Isr. J. Chem.* **2019**, *59*, 892–897.
- [29] a) K. M.-C. Wong, N. Zhu, V. W.-W. Yam, *J. Am. Chem. Soc.* **2002**, *124*, 6506–6507; b) K. M.-C. Wong, W. S. Tang, B. W. K. Chu, N. Zhu, V. W.-W.

- Yam, *Organometallics* **2004**, *23*, 3459–3465; c) W. S. Tang, X. X. Lu, K. M.-C. Wong, V. W.-W. Yam, *J. Mater. Chem.* **2005**, *15*, 2714–2720; d) V. W.-W. Yam, K. H.-Y. Chan, K. M.-C. Wong, N. Zhu, *Chem. Eur. J.* **2005**, *11*, 4535–4543; e) K. M.-C. Wong, W. S. Tang, X. X. Lu, N. Zhu, V. W.-W. Yam, *Inorg. Chem.* **2005**, *44*, 1492–1498; f) H. S. Lo, S. K. Yip, K. M.-C. Wong, N. Zhu, V. W.-W. Yam, *Organometallics* **2006**, *25*, 3537–3540; g) E. C.-H. Kwok, M.-Y. Chan, K. M.-C. Wong, W. H. Lam, V. W.-W. Yam, *Chem. Eur. J.* **2010**, *16*, 12244–12254; h) S. Y.-L. Leung, K. M.-C. Wong, V. W.-W. Yam, *Proc. Natl. Acad. Sci. USA* **2016**, *113*, 2845–2850; i) H.-L. Au-Yeung, S. Y.-L. Leung, V. W.-W. Yam, *CCS Chem.* **2019**, *1*, 464–475; j) S. K.-M. Leung, A. K.-W. Chan, S. Y.-L. Leung, M.-Y. Leung, V. W.-W. Yam, *Chem. Sci.* **2020**, *11*, 499–507; k) K. Zhang, M. C.-L. Yeung, S. Y.-L. Leung, V. W.-W. Yam, *ACS Appl. Mater. Interfaces* **2020**, *12*, 8503–8512.
- [30] a) P. Du, J. Schneider, P. Jarosz, R. Eisenberg, *J. Am. Chem. Soc.* **2006**, *128*, 7726–7727; b) P. Du, K. Knowles, R. Eisenberg, *J. Am. Chem. Soc.* **2008**, *130*, 12576–12577.
- [31] a) D. Zhang, L.-Z. Wu, L. Zhou, X. Han, Q.-Z. Yang, L.-P. Zhang, C.-H. Tung, *J. Am. Chem. Soc.* **2004**, *126*, 3440–3441; b) X. Han, L. Z. Wu, G. Si, J. Pan, Q. Z. Yang, L. P. Zhang, C. H. Tung, *Chem. Eur. J.* **2007**, *13*, 1231–1239.
- [32] K. Zhang, M. C.-L. Yeung, S. Y.-L. Leung, V. W.-W. Yam, *Proc. Natl. Acad. Sci. USA* **2017**, *114*, 11844–11849.
- [33] K. Zhang, M. C.-L. Yeung, S. Y.-L. Leung, V. W.-W. Yam, *J. Am. Chem. Soc.* **2018**, *140*, 9594–9605.
- [34] K. Zhang, M. C.-L. Yeung, S. Y.-L. Leung, V. W.-W. Yam, *Chem* **2017**, *2*, 825–839.
- [35] a) X.-S. Xiao, W. Lu, C.-M. Che, *Chem. Sci.* **2014**, *5*, 2482–2488; b) Y. Chen, C.-M. Che, W. Lu, *Chem. Commun.* **2015**, *51*, 5371–5374; c) M. Krause, D. Kourkoulos, D. González-Abra delo, K. Meerholz, C. A. Strassert, A. Klein, *Eur. J. Inorg. Chem.* **2017**, 5215–5223; d) C. Zou, J. Lin, S. Suo, M. Xie, X. Chang, W. Lu, *Chem. Commun.* **2018**, *54*, 5319–5322; e) J. Chen, L. Ao, C. Wei, C. Wang, F. Wang, *Chem. Commun.* **2019**, *55*, 229–232; f) M. T. Proetto, J. Sanning, M. Peterlechner, M. Thunemann, L. Stegemann, S. Sadeh, A. Devor, N. C. Gianneschi, C. A. Strassert, *Chem. Commun.* **2019**, *55*, 501–504.
- [36] Q. Wan, W.-P. To, C. Yang, C.-M. Che, *Angew. Chem. Int. Ed.* **2018**, *57*, 3089–3093; *Angew. Chem.* **2018**, *130*, 3143–3147.
- [37] Q. Wan, X.-S. Xiao, W.-P. To, W. Lu, Y. Chen, K.-H. Low, C.-M. Che, *Angew. Chem. Int. Ed.* **2018**, *57*, 17189–17193.
- [38] a) K.-H. Wong, K.-K. Cheung, M. C.-W. Chan, C.-M. Che, *Organometallics* **1998**, *17*, 3505–3511; b) V. W.-W. Yam, E. C.-C. Cheng, *Chem. Soc. Rev.* **2008**, *37*, 1806–1813.
- [39] a) W. Lu, K. T. Chan, S.-X. Wu, Y. Chena, C.-M. Che, *Chem. Sci.* **2012**, *3*, 752–755; b) X.-S. Xiao, W.-L. Kwong, X. Guan, C. Yang, W. Lu, C.-M. Che, *Chem. Eur. J.* **2013**, *19*, 9457–9462; c) V. K. Au, N. Zhu, V. W.-W. Yam, *Inorg. Chem.* **2013**, *52*, 558–567; d) K. Yim, E. S. Lam, K. M. Wong, V. K. Au, C.-C. Ko, W. H. Lam, V. W.-W. Yam, *Chem. Eur. J.* **2014**, *20*, 9930–9939; e) K. Yim, V. K. Au, L. Hung, K. M. Wong, *Chem. Eur. J.* **2016**, *22*, 16258–16270; f) K. Yim, V. K. Au, K. M. Wong, V. W.-W. Yam, *Chem. Eur. J.* **2017**, *23*, 5772–5786; g) M.-Y. Leung, S. Y. Leung, K. Yim, A. K.-W. Chan, M. Ng, V. W. Yam, *J. Am. Chem. Soc.* **2019**, *141*, 19466–19478; h) C. Lee, M. Tang, F. K. Kong, W. Cheung, M. Ng, M. Chan, V. W.-W. Yam, *J. Am. Chem. Soc.* **2020**, *142*, 520–529; i) V. W.-W. Yam, A. S. Law, *Coord. Chem. Rev.* **2020**, *414*, 213298; j) D. Zhou, W. To, G. So, M. Tong, G. Cheng, L. Du, D. L. Phillips, C.-M. Che, *Angew. Chem. Int. Ed.* **2020**, *59*, 6375–6382; k) W. Cheung, S. Lai, W. Kwok, M. Tang, C. Lee, M.-Y. Chan, V. W.-W. Yam, *J. Mater. Sci.* **2020**, doi.org/10.1007/s10853-020-04392-1.
- [40] Q. Wan, J. Xia, W. Lu, J. Yang, C.-M. Che, *J. Am. Chem. Soc.* **2019**, *141*, 11572–11582.
- [41] a) C. Mongin, B. Donnio, D. W. Bruce, *J. Am. Chem. Soc.* **2001**, *123*, 8426–8427; b) L. Plasseraud, L. C. Gonzalez, D. Guillon, G. Siss-Fink, R. Deschenaux, D. W. Bruce, B. Donnio, *J. Mater. Chem.* **2002**, *12*, 2653–2658.
- [42] a) M. Chen, C. Wei, J. Tao, X. Wu, N. Huang, G. Zhang, L. Li, *Chem. Eur. J.* **2014**, *20*, 2812–2818; b) M. Chen, C. Wei, X. Wu, M. Khan, N. Huang, G. Zhang, L. Li, *Chem. Eur. J.* **2015**, *21*, 4213–4217; c) N. K. Allampally, M. J. Mayoral, S. Chansai, M. C. Lagunas, C. Hardacre, V. Stepanenko, R. Q. Albuquerque, G. Fernández, *Chem. Eur. J.* **2016**, *22*, 7810–7816.
- [43] a) C. Rest, M. J. Mayoral, K. Fucke, J. Schellheimer, V. Stepanenko, G. Fernández, *Angew. Chem. Int. Ed.* **2014**, *53*, 700–705; *Angew. Chem.* **2014**, *126*, 716–722; b) C. Rest, A. Martin, V. Stepanenko, N. K. Allampally, D. Schmidt, G. Fernández, *Chem. Commun.* **2014**, *50*, 13366–13369; c) V. Stepanenko, R. Kandaneli, S. Uemura, F. Würthner, G. Fernández, *Chem. Sci.* **2015**, *6*, 5853–5858; d) N. Bäumer, K. K. Kartha, N. K. Allampally, S. Yagai, R. Q. Albuquerque, G. Fernández, *Angew. Chem. Int. Ed.* **2019**, *58*, 15626–15630; e) J. P. Coelho, J. Matern, R. Q. Albuquerque, G. Fernández, *Chem. Eur. J.* **2019**, *25*, 8960–8964.
- [44] A. Langenstroer, K. K. Kartha, Y. Dorca, J. Droste, V. Stepanenko, R. Q. Albuquerque, M. R. Hansen, L. Sánchez, G. Fernández, *J. Am. Chem. Soc.* **2019**, *141*, 5192–5200.
- [45] L. Herkert, J. Droste, K. K. Kartha, P. A. Korevaar, T. F. A. de Greef, M. R. Hansen, G. Fernández, *Angew. Chem. Int. Ed.* **2019**, *58*, 11344–11349.
- [46] B. Rytbtchinski, *ACS Nano* **2011**, *5*, 6791–6818.

Manuscript received: March 18, 2020

Revised manuscript received: April 25, 2020

Accepted manuscript online: April 30, 2020